Myotubularin controls desmin intermediate filament architecture and mitochondrial dynamics in human and mouse skeletal muscle

Karim Hnia,[1,2,3,4,5] Helene Tronchère,[6,7] Kinga K. Tomczak,[8,9] Leonela Amoasii,[1,2,3,4,5] Patrick Schultz,[2,3,4,10] Alan H. Beggs,[8] Bernard Payrastre,[6,7] Jean Louis Mandel,[1,2,3,4,5] and Jocelyn Laporte[1,2,3,4,5]

[1]Department of Neurobiology and Genetics, Institut de Génétique et de Biologie Moléculaire et Cellulaire (IGBMC), Illkirch, France. [2]INSERM, U964, Illkirch, France. [3]CNRS, UMR7104, Illkirch, France. [4]Université de Strasbourg, Illkirch, France. [5]Collège de France, chaire de génétique humaine, Illkirch, France. [6]INSERM, U563, Toulouse, France. [7]Université Toulouse III Paul-Sabatier, Centre de Physiopathologie de Toulouse Purpan, Toulouse, France. [8]Division of Genetics and Program in Genomics, Manton Center for Orphan Disease Research, Children's Hospital Boston, Harvard Medical School, Boston, Massachusetts, USA. [9]Division of Pediatric Neurology, Boston Medical Center, Boston University School of Medicine, Boston, Massachusetts, USA. [10]Département de Biologie et Génomique Structurales, IGBMC, Illkirch, France.

Muscle contraction relies on a highly organized intracellular network of membrane organelles and cytoskeleton proteins. Among the latter are the intermediate filaments (IFs), a large family of proteins mutated in more than 30 human diseases. For example, mutations in the *DES* gene, which encodes the IF desmin, lead to desmin-related myopathy and cardiomyopathy. Here, we demonstrate that myotubularin (MTM1), which is mutated in individuals with X-linked centronuclear myopathy (XLCNM; also known as myotubular myopathy), is a desmin-binding protein and provide evidence for direct regulation of desmin by MTM1 in vitro and in vivo. XLCNM-causing mutations in MTM1 disrupted the MTM1-desmin complex, resulting in abnormal IF assembly and architecture in muscle cells and both mouse and human skeletal muscles. Adeno-associated virus–mediated ectopic expression of WT MTM1 in *Mtm1*-KO muscle reestablished normal desmin expression and localization. In addition, decreased MTM1 expression and XLCNM-causing mutations induced abnormal mitochondrial positioning, shape, dynamics, and function. We therefore conclude that MTM1 is a major regulator of both the desmin cytoskeleton and mitochondria homeostasis, specifically in skeletal muscle. Defects in IF stabilization and mitochondrial dynamics appear as common physiopathological features of centronuclear myopathies and desmin-related myopathies.

Introduction

The spatial organization of cells is determined in part by the interaction of organelles with the 3 cytoskeletal systems: intermediate filaments (IFs), microfilaments (MFs), and microtubules (MTs) (1, 2). These systems regulate positioning and movement of organelles in a dynamic manner. Failure of these processes is followed by disruption of polarity and abnormal cellular organization and can be linked to the development and progression of numerous human genetic diseases and cancer (3–5). IFs are cytoskeletal polymers encoded by a large family of differentially expressed genes that provide crucial structural support in the cytoplasm and nucleus of higher eukaryotes. Perturbation of their function accounts for several genetically determined diseases in which cells or organelles are rendered fragile and thus cannot sustain mechanical and nonmechanical stress (6).

During the last decade, studies have shed light on how this structural support is modulated to meet the changing needs of cells and revealed a novel role whereby IFs influence cell growth and death through dynamic interactions with organelles and nonstructural proteins (4). However, few IF-binding proteins have been characterized, and regulation of IF dynamics is poorly understood. Moreover, little is known about the functional significance and tissue specificity of these interactions, owing in part to a lack of useful chemical inhibitors of IFs and their unusual properties and complexity. Skeletal muscle and muscle cells provide a challenging environment in which to decipher the function of IFs and their ability to modulate cellular processes, given their expression redundancy in this tissue and the specific intracellular organization and mechanical constraints of muscle. Desmin represents the major cytoplasmic IF in skeletal muscle. Mutations in desmin (OMIM 601419) or its chaperone protein, αB-crystallin (OMIM 608810), are associated with cardiomyopathy and myopathy, both belonging to the desmin-related myopathy (DRM) and the desmin-related cardiomyopathy (DRCM) subgroups of IF diseases (7). Loss of desmin function (as a result of mutations reported in DRM and DRCM patients) and desmin KO in mice result in decreased number and mislocalization of mitochondria in cardiac and skeletal myocytes (8, 9). A recent study pointed to the cytolinker plectin as the anchor for desmin at the mitochondrial surface (10); however, the functional significance of this scaffold in mitochondrial homeostasis in muscle is not well understood.

Here we report a plectin-independent mechanism in which desmin IFs regulate mitochondrial dynamics and morphology via direct interaction with the phosphoinositide (PI) phosphatase myotubularin (MTM1), which is mutated in the X-linked form

Conflict of interest: The authors have declared that no conflict of interest exists.
Citation for this article: *J Clin Invest.* 2011;121(1):70–85. doi:10.1172/JCI44021.

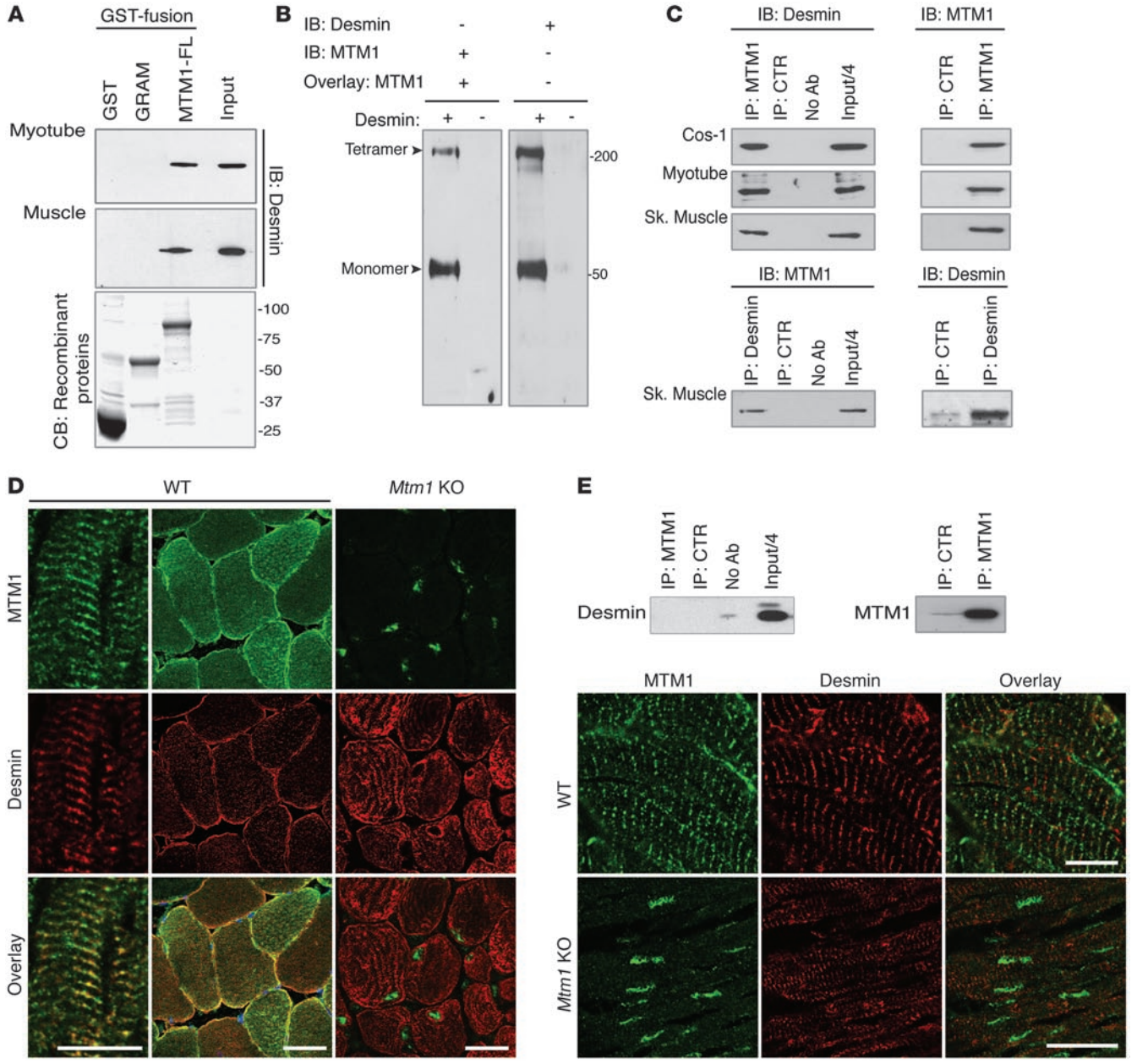

Figure 1

MTM1 interacts with desmin in vitro and in muscle. (**A**) GST–MTM1–full-length (MTM1-FL), GST-MTM1-GRAM PH domain (GRAM), or GST recombinant proteins were incubated with mouse myotube or muscle homogenates. Endogenous desmin interacted with MTM1-FL, but not GST or GRAM. CB, Coomassie blue staining of purified recombinant GST fusions. (**B**) Far-Western blot using recombinant desmin protein overlaid with GST-MTM1-FL and revealed with anti-GST (left) or anti-desmin (right) antibodies. (**C**) Top: co-IP assays with lysates from COS-1 cells (cotransfected with MTM1 and desmin constructs), myotubes, and skeletal muscle using anti-MTM1–specific antibody or a frataxin antibody as a control (CTR). Antibodies used for IB are indicated. Bottom: co-IP of MTM1 with desmin in skeletal (Sk) muscle using the anti-desmin antibody. (**D**) Localization of MTM1 and desmin in WT and *Mtm1*-KO mouse skeletal muscles. Longitudinal and transversal sections showed colocalization of MTM1 and desmin at the z-disc structure and at the sarcolemma. Desmin localization was abnormal in *Mtm1*-KO muscle. Scale bar: 20 μm. (**E**) Desmin did not precipitate with MTM1 in extracts from cardiac muscle. Longitudinal sections of cardiac muscle were stained for MTM1 and desmin. Scale bars: 10 μm.

of centronuclear myopathy (XLCNM; OMIM 310400), a severe congenital myopathy characterized by generalized hypotonia and muscle weakness and absence of cardiac involvement (11–13). MTM1 bound desmin and regulated filament assembly and architecture independently of its enzymatic activity, suggestive of a crucial role for MTM1 in the regulation and/or maintenance of the desmin IF network in skeletal muscle. KO or knockdown (KD) of MTM1 expression and disruption of the MTM1-desmin complex promoted desmin aggregation and led to abnormal mitochondrial positioning, morphology, and dynamics. Furthermore, we found that several XLCNM mutations disrupted the mitochondrial network independently from desmin filaments, which also suggested

a direct implication of MTM1 in mitochondrial dynamics in muscle. We propose, for the first time to our knowledge, a common pathophysiological mechanism between centronuclear and myofibrillar myopathies and underline the importance of MTM1 and the MTM1-desmin complex in the regulation of mitochondrial homeostasis in skeletal muscle.

Results

MTM1 binds desmin IFs in muscle. To decipher the muscle-specific role of MTM1 and the physiopathological mechanisms of XLCNM, we performed a yeast 2-hybrid (Y2H) screen using the *MTM1* sequence as bait against a human fetal and adult skeletal muscle library and isolated 4 different clones encoding portions of the desmin (*DES*) gene transcript. Glutathione S-transferase (GST) pulldown experiments showed that endogenous desmin in mouse C2C12 myotubes and muscle bound specifically to the GST-MTM1 fusion protein (Figure 1A). Results of far-Western blot experiments supported a direct interaction for MTM1 and desmin (Figure 1B). Moreover, using co-IP assays with COS-1, myotube, and skeletal muscle extracts, we confirmed that MTM1 interacted with desmin (Figure 1C). Colocalization experiments in mouse and human skeletal muscles suggested that the molecular association between MTM1 and desmin occurs at the sarcolemma and at the z-disc (Figure 1D and Supplemental Figure 1; supplemental material available online with this article; doi:10.1172/JCI44021DS1), where desmin filaments establish a network to maintain a spatial relationship between the contractile apparatus and organelles and/or plasma membrane. Interestingly, this complex was not detected in cardiac muscle, although both proteins were present (Figure 1E and Supplemental Figure 2A). This is consistent with the lack of evidence for cardiac involvement in *Mtm1*-KO mice and XLCNM patients. Desmin and αB-crystallin expression levels were normal in *Mtm1*-KO cardiac muscle, and desmin was equally distributed between soluble and insoluble fractions (Supplemental Figure 2B). Moreover, H&E staining of cardiac muscle sections showed no myocardial fibrosis (myocyte injury and necrosis) in *Mtm1*-KO mice (Supplemental Figure 2C). In support of this, lactate dehydrogenase (LDH) and creatine kinase (CK) levels were unchanged between WT and *Mtm1*-KO cardiac muscle extracts (Supplemental Figure 2D). Possible cardiac involvement could not be investigated in neonatal cases of XLCNM, as these patients die young. However, several genetically confirmed XLCNM patients who reached adulthood have been previously reported, and none showed signs of cardiomyopathy (Supplemental Table 1).

To define the MTM1-desmin binding domains, we generated MTM1 domains and deletion constructs and also performed alanine scanning. GST pulldown and co-IP assays suggested that the MTM1 region essential for the interaction with desmin is located between residues 160 and 300 (Figure 2A and Supplemental Figure 3, A and B). A structural model was predicted for MTM1 by homology modeling, using the atomic structure of the myotubularin-related protein 2 (*MTMR2*) as a reference (14), and showed that this region contained 4 exposed loops (Figure 2, B and C). We mutated into alanine 5 solvent accessible residues that were located in these loops and potentially implicated in protein-protein interaction: H181, Y206, S209, K255, and K269. When tested by co-IP, these mutations severely or completely disrupted the interaction with desmin (Figure 2B and Supplemental Figure 3C). Overlay assays using synthetic peptides encoding the 4 loops (i.e., MTM1-173-187, MTM1-201-215, MTM1-248-262, and MTM1-264-277) showed that all these loops interacted with desmin (Supplemental Figure 3D). Moreover, interaction between GST-MTM1 and desmin was lost when desmin was preincubated with several competing peptides encompassing the point mutations described above: MTM1-173-(H181A)-187, MTM1-201-(Y206A)-(S209A)-215, or MTM1-248-(K255A)-262. In contrast, the interaction was present, albeit weak, when desmin was mixed with the MTM1-264-(K269A)-277 peptides (Supplemental Figure 3E), which suggests that all 4 loops are required for desmin binding, although the MTM1-264-277 loop appears the most important for the interaction.

The C-terminal part of the 2B rod domain and the N-terminal part of the tail domain (aa 342–456) of desmin were fished out with MTM1 as a bait in Y2H (Figure 2D), which suggests that this region is necessary for MTM1 binding. Using a peptide-mapping strategy, we showed that the aa 352–397 region of desmin bound MTM1 with variable affinity (Figure 2D and Supplemental Figure 3F) and that residues 352–377 displayed the strongest binding to MTM1. Together, these data demonstrated that MTM1 and desmin form a complex through direct interaction in skeletal muscle.

Abnormal desmin filaments in MTM1-deficient cells and muscle. The protein and mRNA expression levels of MTM1 and desmin concomitantly increased during differentiation of myoblasts into myotubes (Supplemental Figure 4A). To address whether MTM1 depletion affects desmin IF dynamics, we monitored desmin expression and localization in myotubes from XLCNM patients, stable *Mtm1*-KD C2C12 cells, and primary *Mtm1*-KO myoblasts. We first validated *Mtm1*-KD C2C12 muscle cells; 3 different clones displayed a strong decrease in MTM1 protein and mRNA levels and 2 clones were comparable to patient myoblasts (Supplemental Figure 4B). Protein and mRNA levels of desmin were increased in patient myoblasts with 3 distinct MTM1 mutations, in *Mtm1*-KD C2C12 cells, in *Mtm1*-KO cells, and in *Mtm1*-KO muscle (Figure 3, A and D, and Supplemental Figure 4C). An approximately 200-kDa band was detected by the desmin antibody specifically in *Mtm1*-KO muscle, potentially representing tetramer detergent-resistant (i.e., insoluble) desmin aggregates (Supplemental Figure 4C). Moreover, desmin aggregates were observed in myotubes and muscle biopsies from 2 XLCNM patients and in isolated muscle fibers and muscles from 2-week-old (i.e., presymptomatic) *Mtm1*-KO mice (Figure 3B and Supplemental Figure 4D). In line with this, a shift in desmin equilibrium from the soluble to the insoluble fraction was observed in *Mtm1*-KD and -KO myoblasts (Figure 3, C and E), indicating a defect in the desmin assembly process.

We next tested the effect of mutations reported in XLCNM or DRM patients on the MTM1-desmin complex. We selected mutations located within the desmin-binding region (MTM1-R184G, MTM1-P205L, and MTM1-R241C) or outside this region (MTM1-R421Q). In addition, we created artificial mutations (MTM1-D278A, MTM1-D380A, and MTM1-C375S) that block the phosphatase activity of MTM1 (12, 13). Our results showed that most patients' mutations abolished the interaction with desmin, whereas the R421Q and dead phosphatase mutants or other artificial mutation (S420D) were capable of binding (Figure 3F). We then tested mutations reported in DRM (DES-N342D, DES-A357P, DES-A360P, and DES-L370P). Far-Western blotting revealed that recombinant MTM1 could bind only WT and the A370P mutant desmin (Figure 3G). Our data suggest that the absence of MTM1 leads to desmin aggregation in muscle cells and tissues and that desmin filament defects play an important role in the physiopathology of XLCNM.

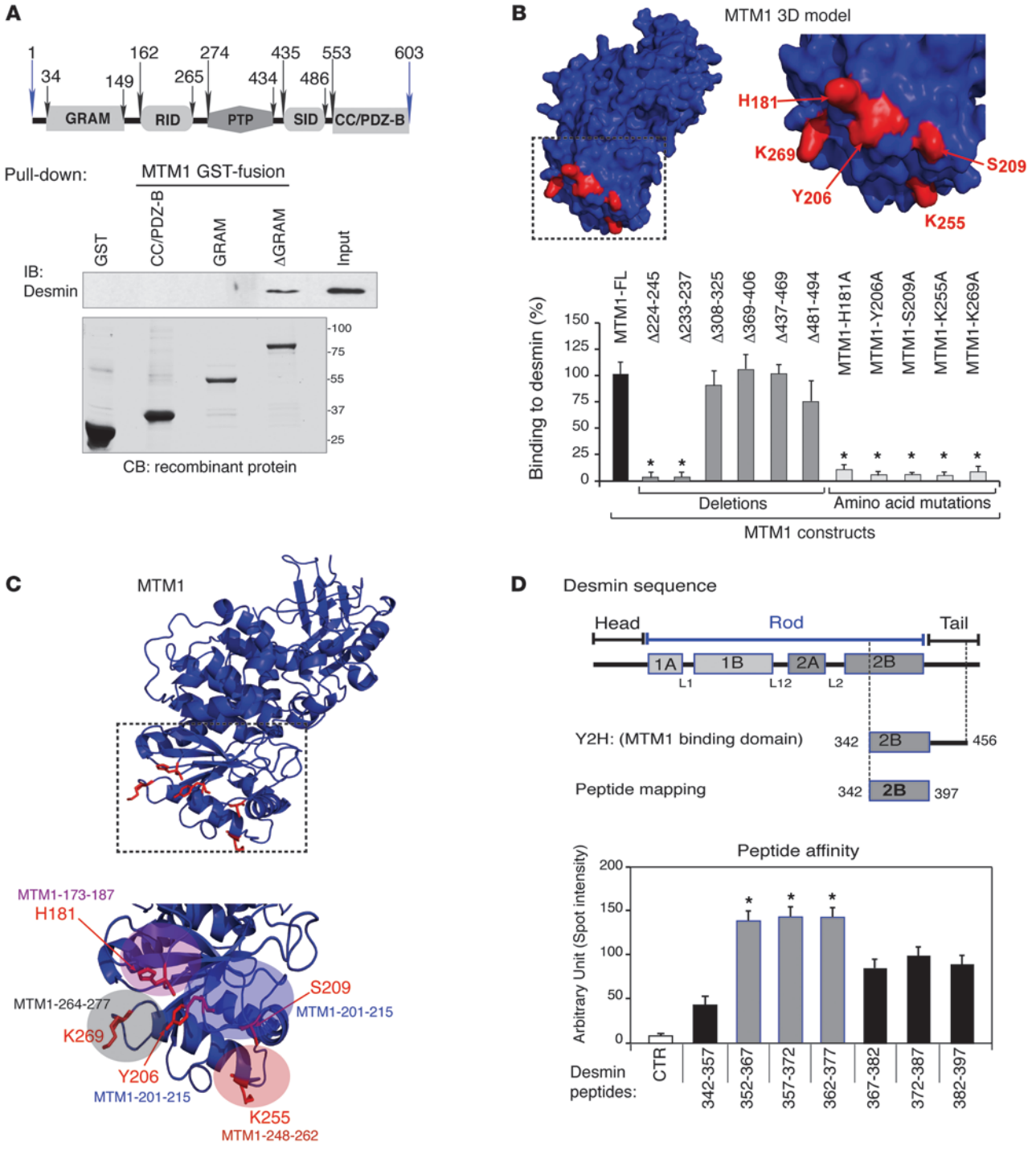

Figure 2

Dissection of the MTM1-desmin interaction. (**A**) Schematic of the MTM1 protein domains. Pulldown of GST-fusion domains of MTM1 with extracts from COS-1 cells overexpressing desmin. Desmin interacted with the ΔGRAM domain. (**B**) Prediction model for MTM1 based on the MTMR2 crystallographic model using PyMol software. The outlined region (shown in detail at right) represents the potential domain for interaction with desmin, composed of 4 independent loops with indicated residues exposed to outside space. aas labeled in red are implicated in desmin binding; histograms represent the relative binding of listed MTM1 constructs (deletion and aa mutation). (**C**) Prediction model for MTM1, showing loops implicated in desmin interaction based on peptide mapping and competition experiments (Supplemental Figure 3, D and E). (**D**) Desmin binding domain. Schematic representation of desmin domains. Dashed lines outline the common region between Y2H clones. The region of desmin implicated in MTM1 binding was determined by peptide mapping experiments. Quantitation of desmin peptides' affinity for MTM1 compared with a non-desmin peptide (CTR). Data were correlated from 3 independent experiments, and statistical analysis of the difference in intensities between positive peptides was set at $^*P \leq 0.05$.

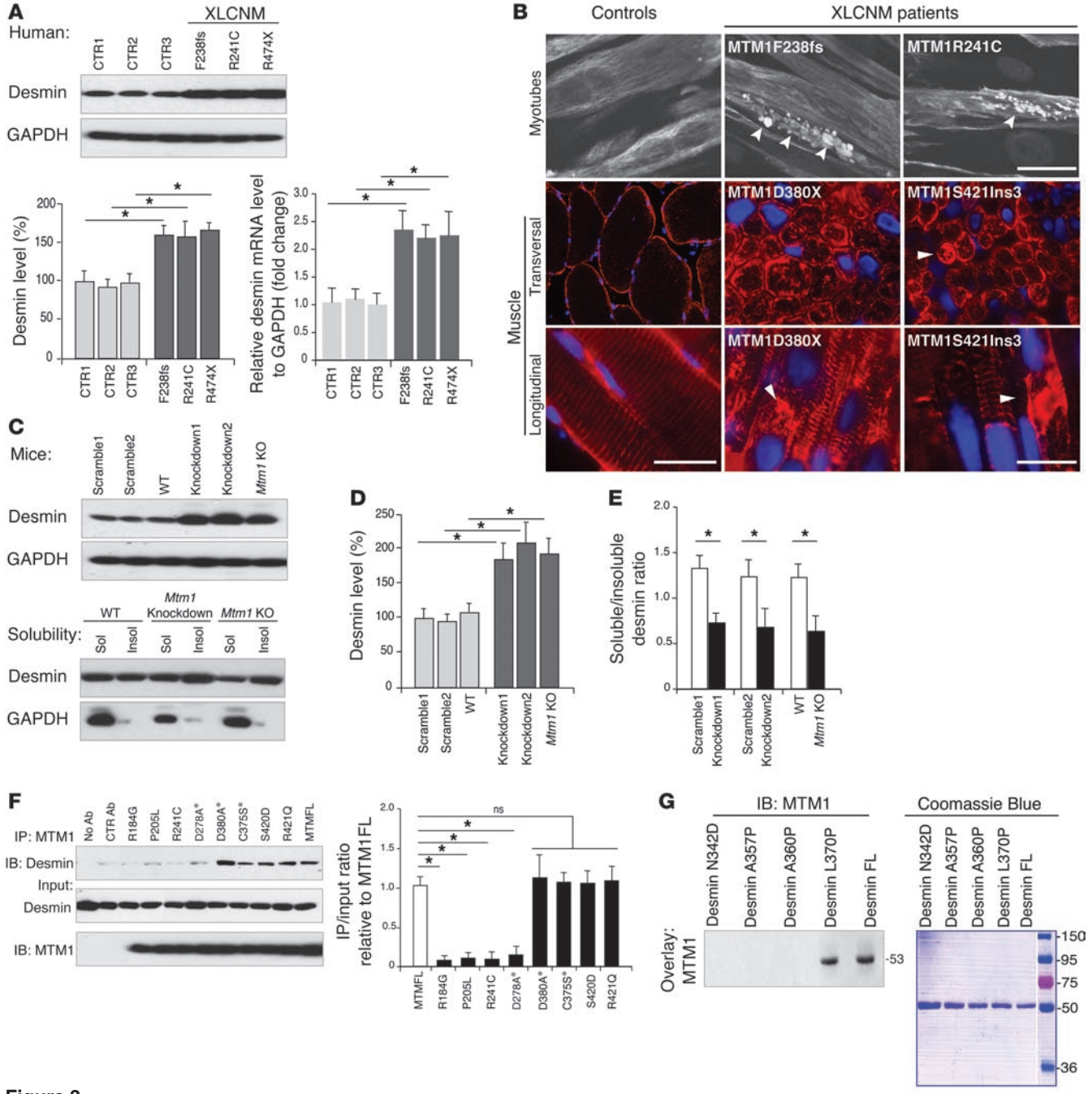

Figure 3

Effect of MTM1 depletion and mutation on desmin expression and localization. (**A**) Desmin was overexpressed in an XLCNM patient's myoblast (R474X, F238 frameshift, and R241C mutations) compared with controls (CTR1–CTR3); corresponding histograms show desmin protein and mRNA levels over 3 independent experiments (*$P \leq 0.05$). (**B**) Desmin aggregation in XLCNM patient myotubes and muscle biopsies. XLCNM mutations are denoted; arrowheads indicate desmin aggregates. Scale bars: 50 μm. (**C**) Effect of *Mtm1*-KD (in C2C12) or -KO background (primary myoblasts from *Mtm1*-KO muscle) on desmin expression and solubility. (**D** and **E**) Quantification of **C**. (**F**) Effect of WT and XLCNM-linked or artificial (asterisks) MTM1 mutations on desmin interaction. Histograms show that several XLCNM mutations located in the interacting domain interfered with desmin binding. Quantification of the level of immunoprecipitated desmin/input relative to control (MTM1-FL) was correlated from 3 independent experiments. *$P \leq 0.05$. (**G**) Effect of DRM-linked desmin mutations on MTM1 binding. Far-Western blot of recombinant WT and mutated desmin using recombinant MTM1 protein for overlay suggested that MTM1 only bound to DES-L370P and WT desmin. Lanes were run on the same gel but were noncontiguous (white line).

Furthermore, the fact that desmin mutations reported in DRM disrupted binding to MTM1 suggests a common molecular mechanism between DRM and XLCNM in skeletal muscle. While desminopathies belong to a genetically heterogeneous group of myofibrillar myopathies with a common pathological pattern of aggregated myofibrillar proteins, we did not observe any abnormal localization of architectural proteins (i.e., α-actinin, titin, and dystrophin) in *Mtm1*-KO muscles (Supplemental Figure 5).

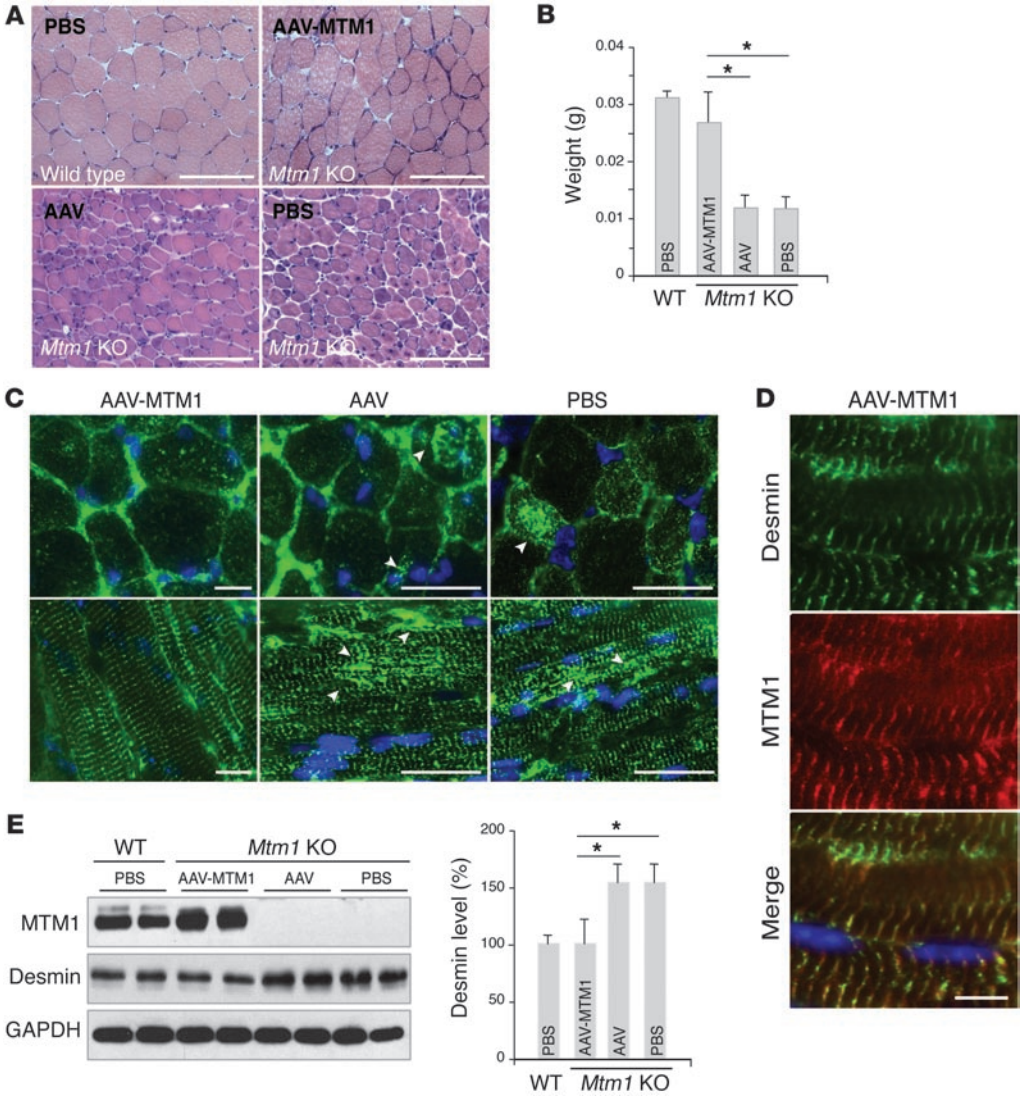

Figure 4
Ectopic expression of MTM1 in *Mtm1*-KO muscle restores normal desmin expression and localization. (**A**) H&E-stained transversal section of tibialis anterior from *Mtm1*-KO muscles injected with AAV-MTM1, AAV, or PBS. AAV-MTM1 rescued muscle fiber atrophy and muscle weight (**B**). Data correlated from 2 independent experiments (n = 6 mice per group). *$P \leq 0.05$. Scale bars: 100 μm. (**C**) Ectopic expression of MTM1 transgene in *Mtm1*-KO muscle restored normal desmin localization in muscle. Arrowheads indicate aggregates of desmin in *Mtm1*-KO muscle injected with AAV or PBS. Scale bars: 50 μm. (**D**) Partial localization (along the z-disc) between MTM1 and desmin in AAV-MTM1–injected muscle. Scale bars: 50 μm. (**E**) Ectopic expression of MTM1 transgene in *Mtm1*-KO muscle restored normal desmin expression level in injected muscles. Data correlated from 2 independent experiments (n = 3 mice per group). *$P \leq 0.05$.

Ectopic expression of the *Mtm1* transgene in *Mtm1*-KO muscle using adeno-associated virus (AAV) rescued muscle pathology and mass (Figure 4, A and B, and ref. 15). Importantly, desmin localization (Figure 4, C and D) and expression (Figure 4E) were also reestablished in muscles injected with MTM1 transgene (AAV-MTM1) compared with controls (empty AAV vector or PBS), suggesting a crucial and direct role of MTM1 in controlling the desmin IF network in skeletal muscle.

MTM1 affects IF assembly and architecture. To further investigate whether MTM1 directly affects desmin assembly, we assessed desmin filament formation in vitro by electron microscopy of negatively stained desmin mixed with recombinant MTM1 proteins in a time-dependent manner (from 10 seconds to 60 minutes). Addition of WT MTM1 led to the formation of abnormally shaped and branched desmin unit length filaments (ULFs) at 10 seconds and irregular filament caliber and ribbon-like filaments at later time points (Figure 5, A and B). In contrast, no effect was noted when the MTM1-S209A mutant, which does not bind desmin, or a control protein were used (data not shown). Addition of MTM1 significantly affected filament width at 5 minutes of assembly (desmin alone, 16.1 ± 2.3 nm; desmin plus MTM1, 13.4 ± 1.9 nm; P = 0.024; Figure 5B). Moreover, MTM1 addition led to irregular filament length at the final steps of filament formation: 2 predominant peaks at 223 ± 25.2 nm and 132 ± 15.5 nm were observed, compared with a unique peak of 222 ± 20.5 nm for desmin alone (Figure 5B). To confirm this effect, we performed cosedimentation experiments by mixing the 2 proteins. Desmin alone polymerized and was entirely found in the pellet fraction, whereas increasing MTM1 concentrations caused a shift of desmin to the soluble (i.e., unpolymerized) fraction (Figure 5, C and D). In parallel, a fraction of GST-MTM1 fusion protein was also shifted to the pellet fraction, which indicates that MTM1 directly binds desmin filaments. However, no change was observed in control assays (GST-MTM1-S209A or GST), in which desmin polymerized and was retrieved in the pellet fraction. The indication that MTM1 affects desmin assembly in a dose-dependent manner was confirmed by monitoring ULF formation in vitro in increasing amounts of MTM1 (Supplemental Figure 6A). Previous data have shown that desmin Ser/Thr phosphorylation can affect its assembly and lead to the collapse and aggregation of filaments. We addressed whether depletion of MTM1 could affect desmin phosphorylation in muscle cells

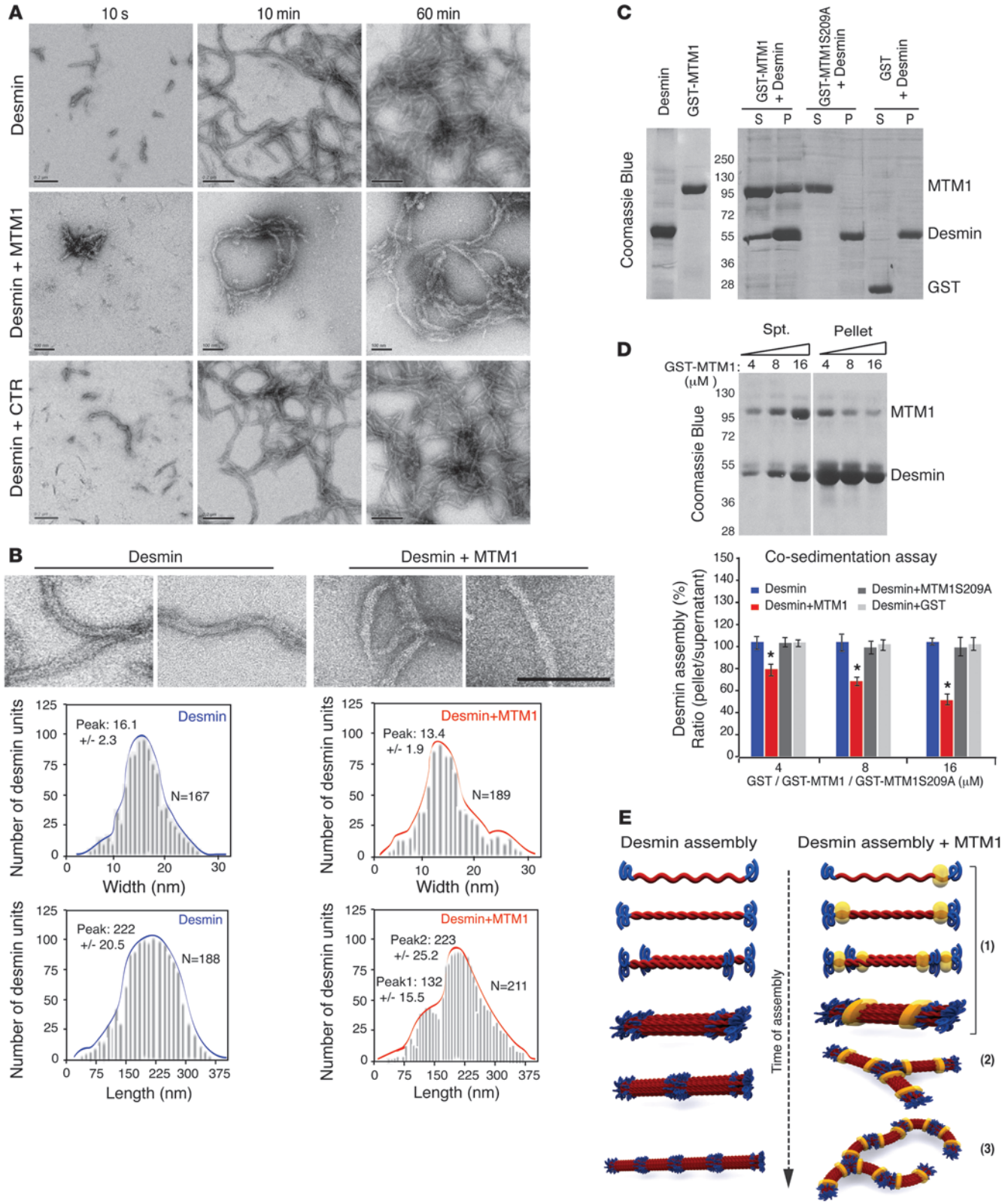
A
10 s
10 min
60 min
Desmin
Desmin + MTM1
Desmin + CTR
B
Desmin
Desmin + MTM1
Number of desmin units
Peak: 16.1
+/- 2.3
N=167
Width (nm)
Peak: 13.4
+/- 1.9
N=189
Peak: 222
+/- 20.5
N=188
Length (nm)
Peak2: 223
+/- 25.2
Peak1: 132
+/- 15.5
N=211
C
Desmin
GST-MTM1
GST-MTM1 + Desmin
GST-MTM1S209A + Desmin
GST + Desmin
S
P
Coomassie Blue
MTM1
Desmin
GST
D
Spt.
Pellet
GST-MTM1: (μM) 4 8 16 4 8 16
Co-sedimentation assay
Desmin assembly (%) Ratio (pellet/supernatant)
Desmin
Desmin+MTM1
Desmin+MTM1S209A
Desmin+GST
GST / GST-MTM1 / GST-MTM1S209A (μM)
E
Desmin assembly
Desmin assembly + MTM1
Time of assembly
(1)
(2)
(3)

Figure 5
Effect of MTM1 on desmin filament polymerization. (**A**) Effect of MTM1 on in vitro assembly of desmin filaments. Assembly of recombinant desmin alone (scale bars: 200 nm) or in the presence of MTM1 WT (scale bars: 100 nm) or the control protein Sumo (scale bars: 200 nm) was monitored by electron microscopy at the indicated times. Addition of WT MTM1 led to irregular and ribbon-like filaments. (**B**) Filament parameters (width and length at 5 minutes of assembly) in the presence or absence of MTM1. Scale bar: 200 nm. (**C**) MTM1 cosedimented with desmin and interfered with polymerization. SDS-PAGE stained with Coomassie blue showed desmin exclusively in the pellet fraction (P; polymerized) in the presence of GST or GST-MTM1S209A, while it was also present in the soluble fraction (S; unpolymerized) in the presence of GST-MTM1. (**D**) Increasing amounts of recombinant GST-MTM1 caused a decrease in desmin polymerization. Lanes were run on the same gel but were noncontiguous (white line). Quantification of desmin assembly (calculated as the ratio of band intensities in pellet/supernatant) in the presence of increasing amounts (4, 8, and 16 μM) of GST-MTM1, GST-MTM1S209A, or GST. Data were correlated from 2 independent experiments. $*P \leq 0.05$. (**E**) Model of MTM1's effect on desmin assembly in vitro. In phase 1 of desmin assembly, 8 tetrameric subunits, made from 2 antiparallel, half-staggered coiled-coil dimers, associate laterally to form ULFs after initiation of assembly. In phase 2, ULFs and short filaments longitudinally anneal to other ULFs. In phase 3, filaments evolve to radial compacted structures. MTM1 addition (yellow) interferes with filament assembly in vitro, leading to a branched-like phenotype at the squiggles step and a ribbon-like structure.

using phospho-Ser/Thr column chromatography enrichment. Our data showed that MTM1 depletion directly affected filament assembly without modifying the phosphorylation level of desmin (Supplemental Figure 6B), as illustrated schematically in Figure 5E. We next tested the ability of WT MTM1 and mutant constructs to restore the desmin filament network in *Mtm1*-KD and -KO myoblasts. Artificial or patient MTM1 mutations within the desmin-interacting domain could not restore normal desmin network; however, WT MTM1 as well as MTM1 containing mutations situated away from this domain reestablished normal desmin filaments (Supplemental Figure 7, A and B, and Supplemental Figure 8A). Moreover, overexpression of MTM1 mutants that do not bind desmin in C2C12 cells (e.g., MTM1-Y206A) strongly disrupted the desmin network (Supplemental Figure 8, B–D), potentially through a dominant-negative effect. In that case, desmin formed aggregates, particularly in the perinuclear region, reminiscent of the *Mtm1*-KD and -KO phenotypes (Supplemental Figure 7B and Supplemental Figure 8B). We concluded that the loss of the MTM1-desmin interaction caused by downregulation or mutation of MTM1 disrupts desmin filaments and promotes their aggregation.

MTM1 PI phosphatase activity is not affected by desmin. It has been established that MTM1 specifically dephosphorylates the D-3 position of phosphatidylinositol 3-phosphate and phosphatidylinositol 3,5-bisphosphate [PtdIns3P and PtdIns(3,5)P_2, respectively], generating PtdIns and PtdIns5P, respectively (12, 13, 16, 17). We addressed a potential effect of desmin on MTM1 PI phosphatase activity. We first observed that the *MTM1* mutations affecting desmin binding (*MTM1*-H181A, *MTM1*-Y206A, *MTM1*-S209A, and *MTM1*-K269A) dephosphorylated PtdIns(3,5)P_2 similarly to the WT protein both in vitro and in vivo (Supplemental Figure 9, A–C). No significant difference in MTM1 phosphatase activity was detected when MTM1 was combined with soluble recombinant desmin or with peptides encoding MTM1-binding sequences of desmin (DES-352-367, DES-357-372, and DES-362-377; Figure 6A). Similarly, the phosphatase activity of MTM1 immunoprecipitated from transfected cells, alone or in combination with desmin, was not significantly modified (Figure 6B). Previous studies have suggested substantial accumulation of MTM1 substrates (PtdIns3P) in *mtm1*-KD zebrafish muscle (18). *Mtm1*-KO and -KD myoblasts displayed marked increases in PtdIns(3,5)P_2 staining compared with control cells (Figure 6C). In addition, we showed that WT MTM1 and MTM1 harboring artificial mutations interfering with desmin binding decreased the endogenous pool of PtdIns(3,5)P_2, consistent with in vitro and ex vivo experiments, whereas XLCNM mutations and the inactive C375S mutant had no effect on PtdIns(3,5)P_2 level (Figure 6D). In a complementary approach, no direct interaction between desmin and PIs or other classes of lipids was observed by fat blot analysis (Supplemental Figure 9D), which suggests that desmin is neither regulated by PIs nor implicated in the regulation of MTM1 PI phosphatase activity. We propose that MTM1 could have 2 independent functions in muscle: as an IF binding/regulating protein, and as a regulator of PI levels in subcellular compartments.

Mitochondrial morphology impairment in MTM1-deficient cells. A connection between IFs and mitochondria was suggested more than 25 years ago. Furthermore, ablation of desmin in mouse or desmin mutations in patients resulted in characteristic alterations in distribution, number, morphology, and respiratory activity of mitochondria (8, 9). Abnormal mitochondrial localization was suspected in XLCNM patients and *Mtm1*-KO muscles (15), but these observations were not characterized further. To address the physiological relevance of the MTM1-desmin partnership, we concentrated on mitochondrial dynamics. In transiently transfected C2C12 muscle, MTM1 mutations that did or did not induce desmin aggregation promoted mitochondrial collapse to the perinuclear region (Figure 7, A and B). Mitochondrial disorganization was also observed in *Mtm1*-KD and -KO cells (Figure 7C), which suggests that depletion or alteration of MTM1 function interferes with normal distribution of mitochondria in muscle cells. In addition, all tested mutations (artificial or reported in XLCNM patients) failed to reestablish the normal mitochondrial network when expressed in *Mtm1*-KD cells (Figure 7D) or in *Mtm1*-KO primary muscle cells (Supplemental Figure 10, A and B). We reported an accumulation of PtdIns(3,5)P_2 in MTM1-deficient cells (Figure 6C) and observed partial colocalization between PtdIns(3,5)P_2 and mitochondria in these cells (in the perinuclear region), which suggests that excess and/or mislocalized PtdIns(3,5)P_2 can affect the mitochondrial network in muscle cells (Supplemental Figure 10C). However, these mutations did not affect MTs and MFs (Supplemental Figure 11). Desmin and mitochondrial collapse were also observed in XLCNM patient cells (MTM1F238fs), *Mtm1*-KD myotubes, and *Mtm1*-KO muscle (Supplemental Figure 12, A–D). Using electron microscopy, we found that the mitochondrial ultrastructure was compromised in *Mtm1*-KD cells (Figure 7E). Mitochondria appeared enlarged with an expanded matrix space, fewer cristae, and less electron-dense staining. Together, these results suggest a role for MTM1 in maintaining the mitochondrial shape and network in muscle cells.

Altered mitochondrial dynamics and function in MTM1-deficient cells. As desmin could be associated with mitochondria, we investigated whether the MTM1-desmin complex can be seen in the mitochondrial fraction. We found MTM1 enriched in this fraction and observed a significant accumulation of desmin in the mitochondrial fraction of *Mtm1*-KO compared with WT muscle (Figure 8, A and B). Because recent studies implicate IFs in mitochondrial

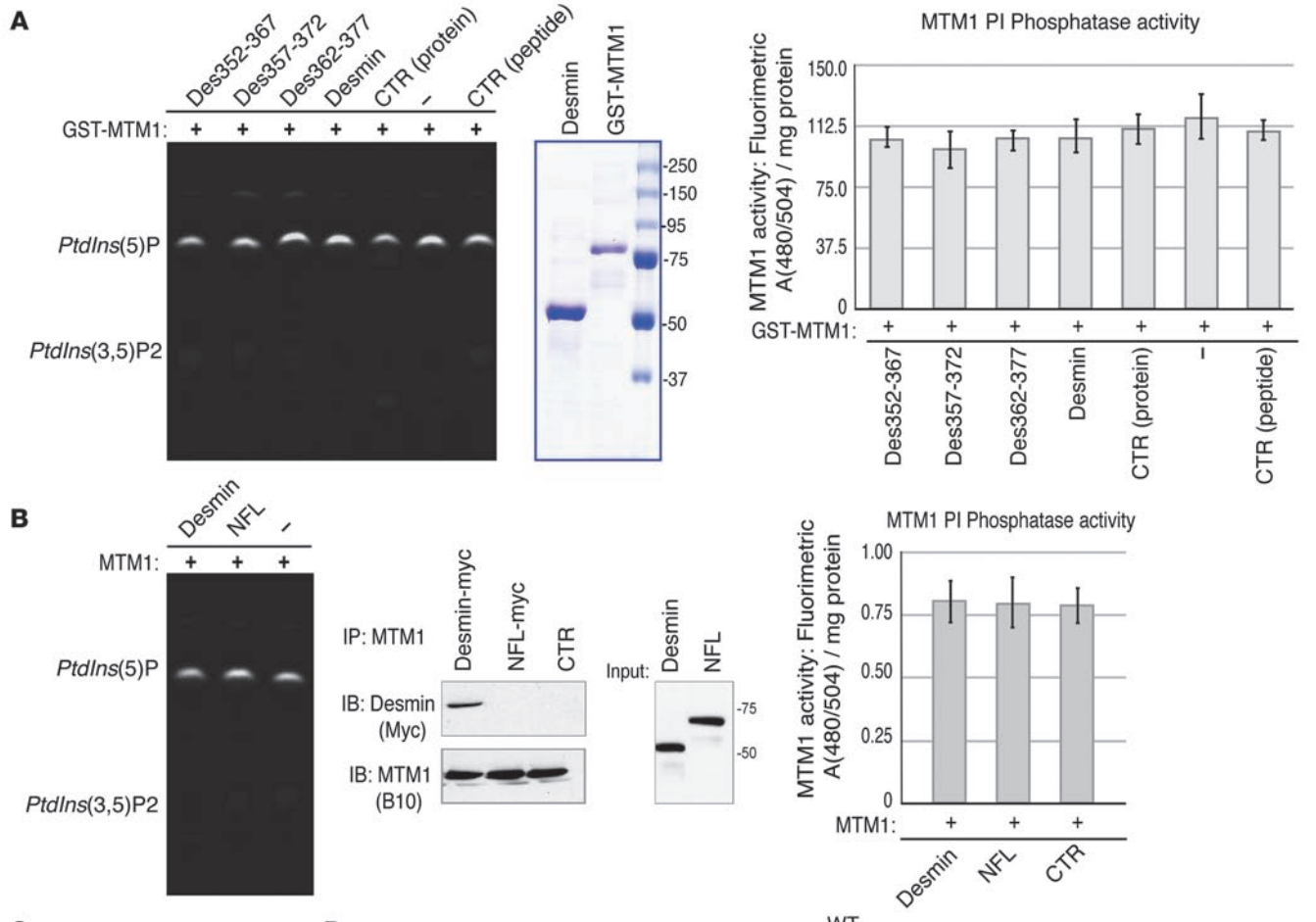
A
Des352-367
Des357-372
Des362-377
Desmin
CTR (protein)
–
CTR (peptide)
GST-MTM1:
PtdIns(5)P
PtdIns(3,5)P2
Desmin
GST-MTM1
250
150
95
75
50
37
MTM1 PI Phosphatase activity
MTM1 activity: Fluorimetric A(480/504) / mg protein
150.0
112.5
75.0
37.5
0
B
Desmin
NFL
–
MTM1:
IP: MTM1
Desmin-myc
NFL-myc
CTR
IB: Desmin (Myc)
IB: MTM1 (B10)
Input:
MTM1 PI Phosphatase activity
1.00
0.75
0.50
0.25
C
PtdIns(3,5)P2
WT
KO Mtm1
Scramble
Mtm1 knockdown
D
WT
MTM1K255A
MTM1S209A
MTM1FL
MTM1P205L
MTM1R241C
MTM1C375S
PtdIns(3,5)P2 level
Relative fluorescence
Wild type
KO Mtm1
MTM1FL
MTM1H181A
MTM1Y206A
MTM1S209A
MTM1K255A
MTM1K269A
MTM1C375S
MTM1R184G
MTM1P205L
MTM1R241C
MTM1R421Q
No transfection
Artificial mutations
XLCNM mutations

Figure 6
Effect of desmin on MTM1 PI phosphatase activity. (**A**) GST-MTM1 recombinant proteins were incubated with PtdIns(3,5)P_2 alone or in the presence of full-length desmin or specified desmin peptides (versus Sumo as a control protein and control peptide, respectively). No significant variation in the PtdIns5P/PtdIns(3,5)P_2 ratio per mg protein was observed after quantification. Coomassie blue gel of purified GST-MTM1 and desmin are also shown. (**B**) Immunoprecipitated MTM1-containing complexes from cells cotransfected with MTM1-B10 and desmin-myc or with MTM1-B10 and NFL-myc (neurofilament light chain) were incubated with PtdIns(3,5)P_2. Immunoprecipitated complexes were confirmed by Western blot analysis with anti-B10 and anti-myc antibodies. No significant changes in MTM1 phosphatase activity were found by quantification of the PtdIns5P/PtdIns(3,5)P_2 ratio. (**C**) Immunolabeling of MTM1 substrate in *Mtm1*-KO and -KD cells showed accumulation of PtdIns(3,5)P_2 compared with control cells. Single cells are outlined (original magnification, ×63). (**D**) MTM1 mutations within the desmin-binding domain (e.g., MTM1K255A and MTM1S209A) did not interfere with MTM1 PI phosphatase activity in cells, but XLCNM mutations (e.g., MTM1R241C and MTM1R421Q) or the catalytic inactive mutation (MTM1C375S) significantly impaired this activity. Single cells are outlined (original magnification, ×63). Histograms represent fluorescent intensities of PtdIns(3,5)P_2 over 2 independent experiments. *$P \leq 0.05$.

transport (19), we asked whether MTM1 depletion in muscle cells could affect mitochondrial motility and velocity in addition to their localization and morphology. Overall mitochondrial motility was similar between *Mtm1*-KD and control muscle cells, as assessed by randomly counting motile mitochondria throughout the cells (Figure 8, C–E, and Supplemental Movies 1 and 2). However, closer analysis revealed that although perinuclear mitochondria were less motile, the motility of mitochondria in the cell periphery increased in *Mtm1*-KD compared with control cells (Figure 8C). To further confirm these results, we tracked individual mitochondria and measured their velocity. Again, we observed a significant decrease in the average velocity of perinuclear mitochondria in *Mtm1*-KD compared with control cells (*Mtm1*-KD, 0.12 ± 0.03 μm/s; control, 0.22 ± 0.02 μm/s; $P = 0.024$, Student's *t* test), whereas the average velocity of mitochondria at the cell periphery was higher compared with control cells (*Mtm1*-KD, 0.31 ± 0.04 μm/s; control, 0.23 ± 0.03 μm/s; $P = 0.027$, Student's *t* test; Figure 8, D and E). Recently, Winter et al. proposed that the link between mitochondria and desmin occurs via the IF-based cytolinker plectin isoform 1b (Plectin1b) and that this interaction affects the shape and function of mitochondria (10). We tested whether MTM1 depletion in muscle affects this partnership. The amount of co-IP of desmin with the cytolinker plectin did not change in the mitochondrial or microsomes fractions isolated from *Mtm1*-KO muscle (Figure 8F), which suggests that the plectin-desmin interaction is not affected in *Mtm1*-KO muscle. As mitochondria fission/fusion homeostasis may affect mitochondrial ultrastructure, we recorded mitochondrial fission/fusion events in *Mtm1*-KD cells by confocal time-lapse microscopy and did not find any differences compared with control cells (Supplemental Figure 13A). We next investigated mitochondrial function in *Mtm1*-KD cells and in primary muscle cells from 4 XLCNM patients. A significant decrease in cytochrome *c* oxidase activity was observed in both cell types and in *Mtm1*-KO muscle (Figure 9A and data not shown). We also observed a decrease in the ATP content of *Mtm1*-KO muscle (Figure 9B), which suggests that alteration of mitochondrial function in cells lacking MTM1 may promote hypotonia in XLCNM muscle. As calcium homeostasis defects have been recently reported in *Mtm1*-KO muscle (20), we investigated whether this defect is linked to mitochondrial dysfunction by monitoring the mitochondrial permeability transition (MPT) from *Mtm1*-KO muscle. No significant difference between *Mtm1*-KO and WT mitochondria was observed in terms of membrane susceptibility to Ca^{2+} (Figure 9, C and D). No differences in mitochondrial membrane potential were observed when the JC-1 stain was used (Supplemental Figure 13B). Disruption of mitochondrial dynamics may be linked to apoptotic events (21); however, TUNEL experiments revealed no significant alteration in level of apoptosis in *Mtm1*-KD muscle cells compared with control cells (Figure 9E). Moreover, *Mtm1*-KD and control cells have a similar number of nuclei with condensed/fragmented DNA following staurosporine treatment (Supplemental Figure 13C).

Discussion

We have identified MTM1 as an IF-binding protein and present evidence herein for MTM1-based regulation of desmin IF and mitochondrial dynamics in muscle cells. MTM1 bound directly to desmin and affected filament assembly in vitro and architecture in vivo. Molecular dissection of the interaction defined the Rac1-induced recruitment domain of MTM1 (22) and the 2B rod domain of desmin as the molecular interface. Several mutations leading to XLCNM and DRM, respectively, are located to these domains (23–25), highlighting the importance of this complex in skeletal muscle. Analysis of the 2B rod domain of desmin has attracted much attention, since a number of desmin mutations occur in this region, and it has previously been implicated in filament assembly (26). As excess MTM1 led to abnormal shape and branching of desmin filaments in vitro, it is possible that MTM1 binding to desmin affects the structure of newly formed filaments. These abnormal filaments are similar to those formed in the presence of a mutated (R120G) αB-crystallin (27). This gain-of-function R120G mutation in αB-crystallin also leads to desmin aggregation and to a DRCM (28). Previous studies indicate that the YRKLLEGEE motif of desmin (DES-403-410) is crucial for the formation of authentic tetrameric complexes and for the control of filament width, rather than elongation, during assembly (29). MTM1 binding to the DES-352-377 region (adjacent to the YRKLLEGEE motif) may regulate the formation and/or turnover of desmin filaments in muscle cells. Moreover, Colakoglu and Brown proposed a mechanism, termed *intercalary subunit exchange*, for vimentin and neurofilaments in cells (30). They showed that IF subunits incorporate along the length of filaments without compromising interaction among other subunits, leading to a unique turnover and alteration of IF polymer composition. The implication of IF-binding proteins, such as MTM1 or αB-crystallin, in this process remains to be evaluated.

IFs have a well-established role as major mechanical integrators of cells and tissues. This function is mainly attributed to their unique viscoelastic properties that render them more resistant to deformation under mechanical stress (31). In addition to their unusual viscoelasticity, IFs also exhibit highly dynamic properties in vivo. The concept that the binding of proteins influences MF and/or MT dynamics by exploiting the intrinsic structural plasticity of the filaments currently extends to IFs, as more IF-binding proteins are being discovered. IFs also appear to be involved in the distribution of membrane-bound organelles (32). Although the transport of membranous organelles is mainly mediated by molecular motors and their respective cytoskeletal tracks, their proper

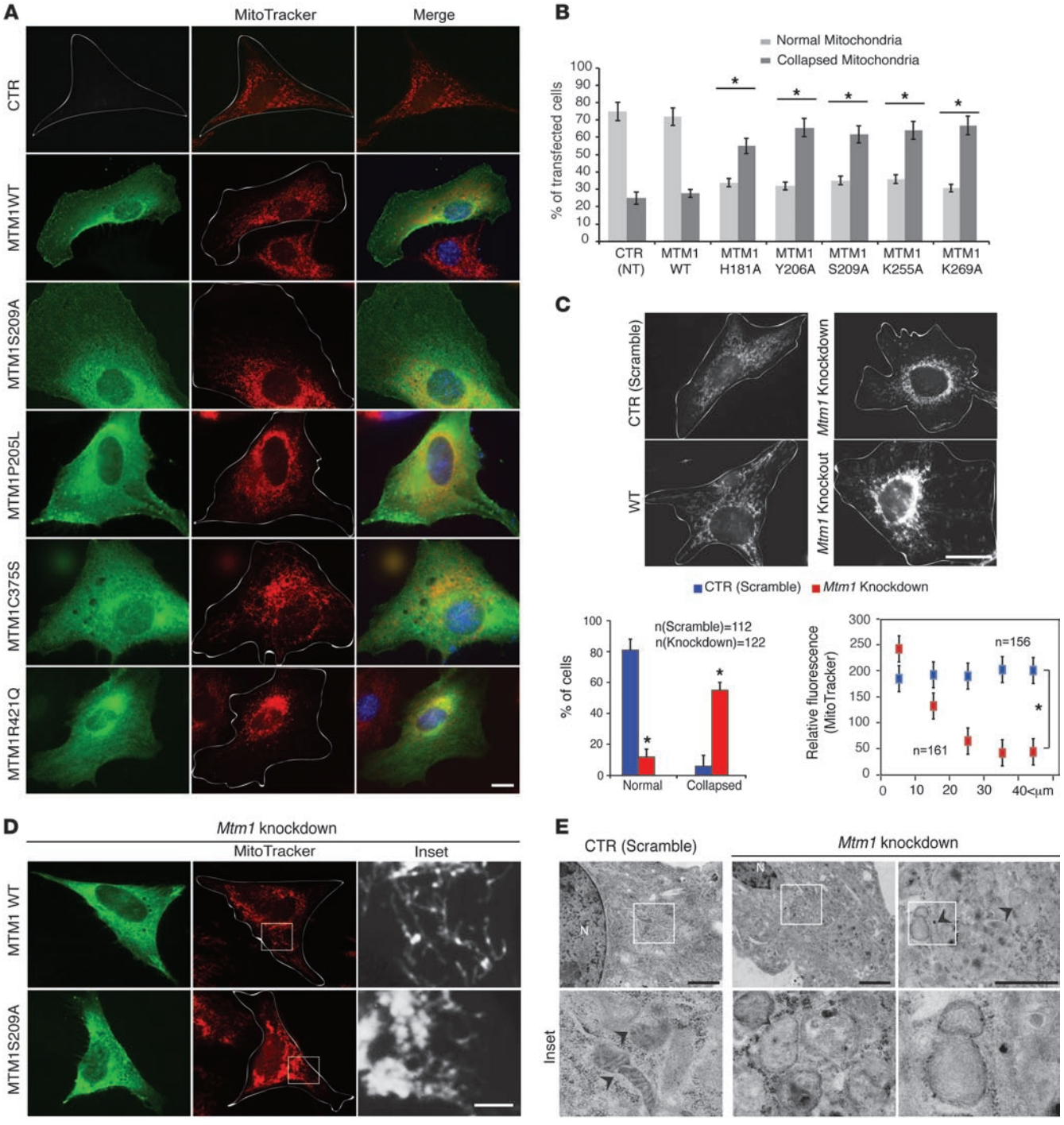

Figure 7

MTM1 has a role in mitochondrial dynamics in muscle cells. (**A**) Effect of MTM1 mutations on mitochondrial morphology in C2C12 cells. Single cells are outlined. Scale bar: 10 μm. (**B**) Quantitation of mitochondrial phenotypes observed as normal or collapsed. More than 100 cells per transfection were counted for 2 independent experiments. Nontransfected (NT) cells served as a control. *$P \leq 0.05$. (**C**) Confocal microscopy images after MitoTracker Red staining showed accumulation/collapse of mitochondria at the perinuclear region in *Mtm1*-KO and -KD myoblasts. Scale bar: 20 μm. Also shown is quantitation of mitochondrial phenotypes observed over 2 independent experiments, as well as position of mitochondria with respect to nuclei (0 μm) in control and *Mtm1*-KD C2C12 cells. *$P \leq 0.05$. (**D**) Overexpression of MTM1-WT, but not MTM1-S209A, in *Mtm1*-KD cells restored mitochondrial morphology. Single cells are outlined (original magnification, ×63). Boxed regions are shown at higher magnification at right (scale bar: 10 μm). (**E**) Ultrastructural observations of *Mtm1*-KD cells by electron microscopy revealed the presence of swollen mitochondria (arrowheads). Boxed regions are shown at higher magnification below (original magnification, ×20,000). Scale bars: 1 μm.

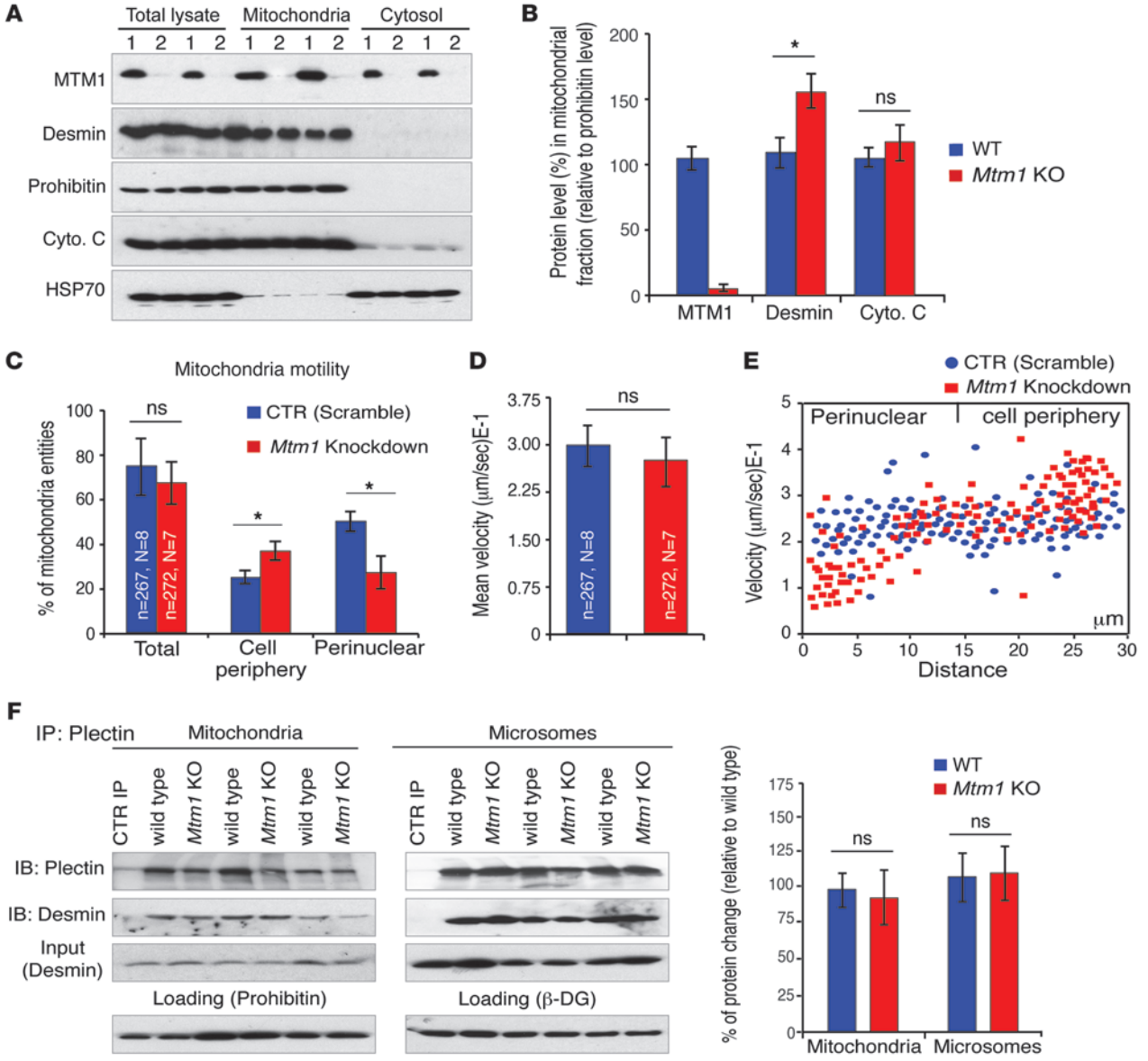

Figure 8

The MTM1-desmin complex is associated with mitochondria and is involved in mitochondrial dynamics/motility. (**A**) Subcellular fractionation of muscles from WT or *Mtm1*-KO mice (lanes labeled 1 and 2, respectively) showed accumulation of desmin in the mitochondrial fraction in *Mtm1*-depleted muscle along with the mitochondrial markers prohibitin and cytochrome *c*. The cytosolic protein HSP70 served as a control. (**B**) MTM1, desmin, and cytochrome *c* levels in mitochondrial fractions in WT and *Mtm1*-KO muscle relative to the mitochondrial protein (prohibitin). Data correlated from 2 independent experiments (3 mice per group; 2 tibialis anterior muscles per mouse). *$P \leq 0.05$. (**C**) Number of motile mitochondria in the peripheral and perinuclear region of scramble and *Mtm1*-KD myoblasts. *$P \leq 0.05$. (**D**) Mean velocity of mitochondria in scramble versus *Mtm1*-KD myoblasts. (**C** and **D**) N, number of total cells monitored; n, number of mitochondria scored. (**E**) Spot plot depicting velocity of individual mitochondria and their cellular position in relation to nucleus (0 μm) in scramble and *Mtm1*-KD myoblasts. Data correlated from 2 independent experiments. (**F**) Depletion of MTM1 in muscle did not affect the plectin-desmin interaction. Mitochondrial and microsomal fractions from WT and *Mtm1*-KO muscles were subjected to IP with an anti-plectin antibody and revealed by anti-desmin antibody. Prohibitin and β-DG were used as mitochondrial and microsomal markers, respectively. Data were correlated from 2 independent experiments. *$P \leq 0.05$.

positioning in the cytoplasm frequently appears to involve interactions with IFs. IFs have been recently implicated in organelle transport and particularly in mitochondrial trafficking (33). They are believed to be involved in anchoring mitochondria at sites of high energy demand or in the vicinity of other organelles to allow for effective signaling. Indeed, loss of desmin (8) or MTM1 in muscle cells (present study) has been shown to lead to mitochondrial positioning and dynamics defects. IFs may also directly influence mitochondrial membrane behavior by supporting proper protein and lipid targeting. Loss of accurate mitochondrial positioning in desmin-null cardiomyocytes leads to loss of proximity to other organelles, including the myofibrillar contractile apparatus and the endoplasmic/sarcoplasmic reticulum (8). In *Mtm1*-KD and -KO cells, and in cells in which MTM1-desmin interaction is disrupted

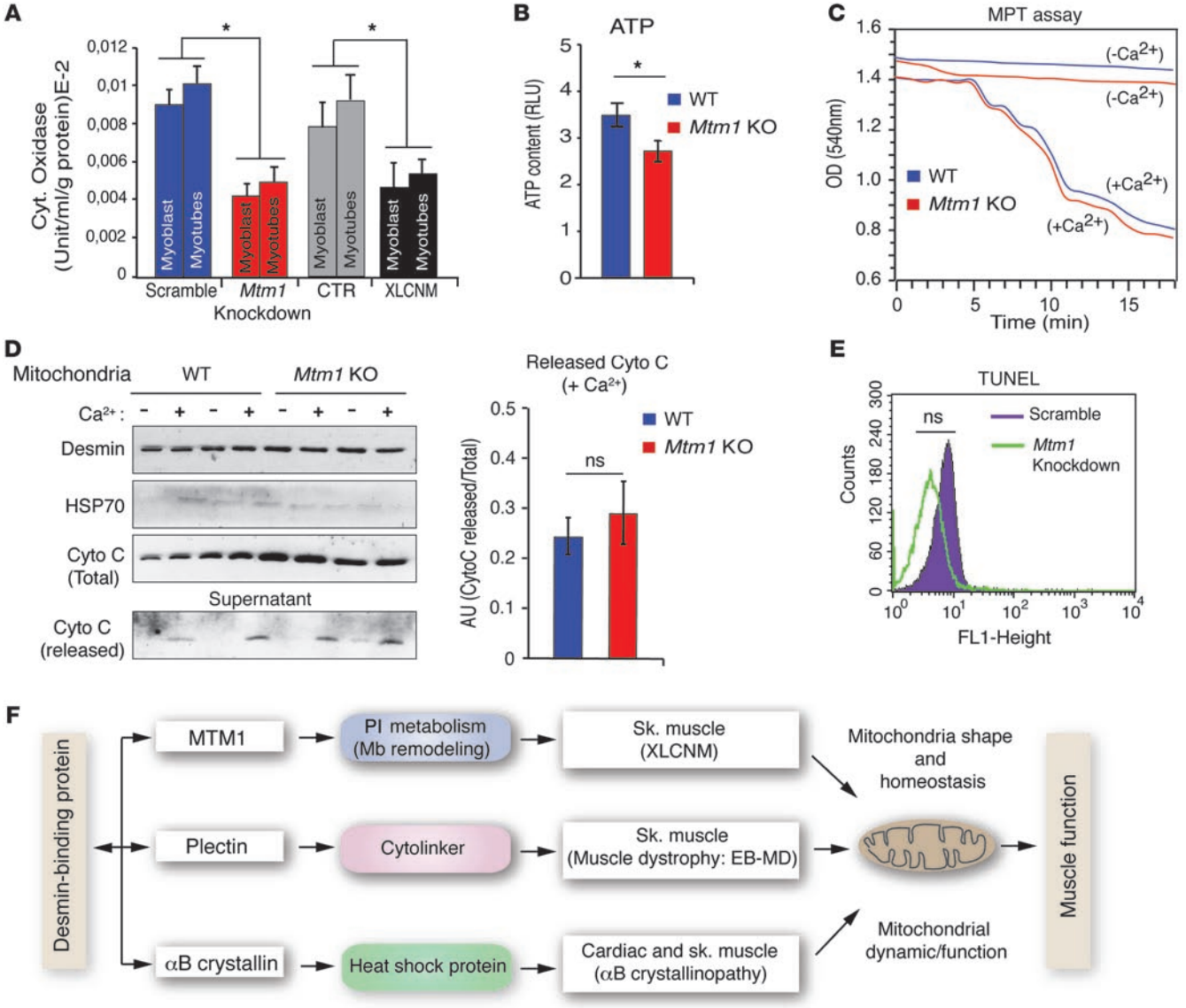

Figure 9

Involvement of MTM1 in mitochondrial function and homeostasis in muscle. (**A**) Decreased cytochrome oxidase activity in *Mtm1*-KD C2C12 and XLCNM patient myoblasts and myotubes. Cell lines from 3 XLCNM patients were assayed. 3 independent experiments were analyzed. $*P \leq 0.05$. (**B**) ATP content of total muscle homogenates from WT and *Mtm1*-KO mice. $*P \leq 0.05$. (**C**) Mitochondria freshly isolated from mouse muscle were used to measure Ca^{2+}-induced MPT. Changes observed during the 18-minute period are shown for WT and *Mtm1*-KO mitochondria in the presence and absence of Ca^{2+}. (**D**) Cytochrome *c* release was monitored from freshly isolated mitochondria from WT and *Mtm1*-KO muscles. Mitochondria were incubated with or without Ca^{2+}, followed by analysis of cytochrome *c* released to the supernatant. (**B**–**D**) Data were correlated from 2 independent experiments (3 mice per group; 2 tibialis anterior muscles per mouse). (**E**) Decreased MTM1 levels did not enhance apoptotic events. TUNEL assay was used to determine the apoptotic rate of control and *Mtm1*-KD cells. FACS analysis showed no significant difference in the profile of control and KD samples. Data are representative of 3 independent experiments. (**F**) Diagram illustrating IF-binding proteins and their associated diseases together with potential connection to mitochondrial dynamics and function. EB-MD, epidermolysis bullosa with muscular dystrophy; Mb, membrane.

(overexpression of MTM1 mutants with a dominant-negative effect), both mitochondria and IFs accumulated at the perinuclear region. Mitochondrial collapse was observed even in the case of XLCNM mutations that have maintained their ability to bind desmin, which suggests that MTM1 has a direct, non–desmin-dependent role in mitochondrial dynamics/homeostasis in muscle. In *Mtm1*-KD cells, the accumulated mitochondria in the perinuclear compartment were less dynamic compared with mitochondria at the periphery of the cells or in the perinuclear regions of control cells. IF collapse or/and excess of PIs (e.g., PtdIns[3,5]P_2) in the absence of MTM1 may render mitochondria less motile and compromised. In addition, we observed an increased association of desmin to mitochondria in *Mtm1*-KO compared with WT muscle. To describe the involvement of MTM1 and desmin in mitochondrial dynamics, 2 distinct — although complementary — mechanisms could be proposed. The first implicates IF-binding proteins, which

are able to affect IF dynamics at the structural level. The second implicates plectin as a cytolinker between IFs and mitochondria. Indeed, plectin deficiency causes detachment of desmin IFs from the z-disc, costameres, mitochondria, and nuclei, promoting the formation of desmin aggregates. The potential interconnections between these 2 pathways should be investigated, in particular the functional link among plectins, myotubularin, and αB-crystallin and how they influence desmin filaments.

Several findings support a role for myotubularin in membrane trafficking through its role in PI metabolism (34, 35). PtdIns3P and PtdIns(3,5)P_2, the substrates of myotubularin, are primarily localized to the membrane of early and late endosomes, respectively, and studies have implicated myotubularin family members in endosomal trafficking events and membrane homeostasis (36, 37). However, desmin did not affect in vitro or ex vivo MTM1 phosphatase activity, and MTM1 mutants that cannot bind desmin were as enzymatically active as the WT protein (Supplemental Figure 9), which suggests that IFs do not interfere with or modulate MTM1 activity. However, it is possible that desmin plays a role in stabilizing MTM1 association to organelles. MTM1 might have 2 distinct roles. One is to regulate vesicle trafficking and maturation, but also positioning of organelles, such as mitochondria, through the tight regulation of the PI pool in the cell. A second role for MTM1 — likely PI independent — is the regulation of IFs (Figure 9F).

In normal skeletal muscle, MTM1 colocalized with desmin at the sarcolemma and also at the z-disc. However, in cardiac muscles, no interaction was evident by biochemical approaches, and weaker colocalization was observed for MTM1 and desmin. While desmin mutations have been associated with both cardiomyopathy and myopathy, cardiac involvement is not a common sign of adult XLCNM patients (38). We also found no alteration in the histology of cardiac muscle in the *Mtm1*-KO mice. Together, these observations point to a specific role for the MTM1-desmin complex in skeletal muscle.

Mitochondrial aggregates have been observed both in *Des*-KO mice and in DRM biopsies (8, 39). Mitochondrial abnormalities can be detected very early, before other structural defects become obvious. The observed alterations are frequently associated with swelling and degeneration of the mitochondrial matrix. In addition, transgenic mice carrying the *Des* L345P missense mutation are characterized by striking abnormalities in mitochondrial morphology and Ca^{2+} handling (9). Recent findings also demonstrate substantial deregulation of Ca^{2+} handling and homeostasis in *Mtm1*-KO mouse and *mtm1*-KD zebrafish muscle, paralleled by the disruption of excitation-contraction coupling linked to T-tubule abnormalities (18, 20). Combined with our findings of abnormal mitochondrial morphology and positioning in cells expressing MTM1 mutants and in *Mtm1*-KD cells, these observations lead us to postulate that deregulation of Ca^{2+} handling in MTM1 deficiency is caused both by triad disorganization and by a mitochondrial homeostasis defect. As centralization of nuclei is a hallmark of centronuclear myopathy, and as an increased number of internal nuclei is also observed in DRM and *Des*-KO mice (24), we envisage a more general implication of the MTM1-IF complex in organelle positioning.

In summary, we present evidence that MTM1 regulates desmin IF assembly and mitochondrial positioning and dynamics in skeletal muscle cells. We propose that defective mitochondrial homeostasis is a common physiopathological feature of centronuclear myopathies and desmin-related myopathies.

Methods

Study approval. Care and manipulation of mice was performed in accordance with national and European legislations on animal experimentation and was approved by the Com'Eth (Ethical committee for animal experimentation, IGBMC, Strasbourg, France). Studies using human cells and tissues were authorized by the "Comité d'éthique des Facultés de Médecine, d'Odontologie et de Pharmacie de Strasbourg" (Strasbourg, France), and all study participants provided informed consent.

Y2H. Y2H screening was performed by Hybrigenics Inc. using aa 146–603 of human MTM1 as bait. A human adult/fetal skeletal muscle cDNA library (Hybrigenics Inc.) was used to screen for potential MTM1 interactors.

Antibodies. Antibodies against MTM1 used in this study were the 1G1 and R2347 antibodies (15, 22) and novel polyclonal antibodies against the human MTM1 C-terminus (SQMMPHVQTHF) and the mouse MTM1 C-terminal end (TSSSSQMVPHVQTHF). Monoclonal anti-titin, anti-myotilin, and anti-plectin and polyclonal anti-dystrophin, anti-utrophin, anti–β-dystroglycan (β-DG), and anti-syncoilin antibodies were a gift from D. Mornet (INSERM ERI25, Montpellier, France). Commercial antibodies used in this study are detailed in Supplemental Methods.

GST pulldown and co-IP assays. MTM1 recombinant proteins were produced in the BL21-Rosetta 2 strain (Novagen); GST fusion proteins were purified and coupled to glutathione sepharose beads (see Supplemental Methods). COS-1 or SW13vim cells were transiently transfected with pcDNA3.1-desmin construct for 24 hours and homogenized in ice-cold lysis buffer (10 mM Tris-Cl, pH 7.6; 140 mM NaCl; 5 mM EDTA; 5 mM EGTA; 0.5% [v/v] Triton X-100; and 2 mM PMSF). Homogenates were incubated with GST fusion proteins coupled to beads, and interacting proteins were analyzed by Western blot. For co-IP experiments, fresh murine tibialis anterior muscles were dissected and homogenized with a dounce homogenizer in ice-cold co-IP buffer (50 mM Tris-Cl, pH 7.5; 100 mM NaCl; 5 mM EDTA; 5 mM EGTA; 1 mM DTT; 0.5% Triton X-100; and 2 mM PMSF) supplemented with 0.05% (w/v) SDS. For muscle microsomal fraction, pooled muscles were treated as described previously (40). Lysates were precleared with 50 μl of G-sepharose beads (GE Healthcare) and subsequently incubated with antibodies of interest for 12–24 hours at 4°C. Protein G-sepharose beads (50 ml) were then added for 4 hours at 4°C to capture the immune complexes. Resulting immune-bound complexes were eluted in Laemmli buffer and submitted to SDS-PAGE and Western blot analysis.

Desmin purification, electron microscopy, and cosedimentation assay. Recombinant desmin was expressed and purified according to specifications of Herrmann et al. (41, 42); see Supplemental Methods for details. To visualize desmin filaments, recombinant proteins were solubilized at 0.4 mg/ml in solubilization buffer (5 mM Tris-HCl, pH 8.4; 1 mM EDTA; 0.1 mM EGTA; and 1 mM DTT), and assembly was initiated by addition of an equal volume of assembly buffer (45 mM Tris-HCl, pH 7.0; and 100 mM NaCl). Filaments were deposited onto a glow-discharged, carbon-coated copper electron microscopy grid (29), stained with 2% uranyl acetate, and observed under a Philips CM120 transmission electron microscope equipped with a LaB6 filament and operating at 100 kV. MTM1 recombinant protein was added before desmin polymerization (equimolar mixture or with increasing MTM1 molarities), and desmin assembly was started by diluting the mixture in the assembly buffer. The effect of MTM1 on desmin assembly was also investigated by sedimentation, as described previously (43).

Cell culture and immunofluorescence. Culture and transfection procedures of COS-1 and C2C12 are detailed in Supplemental Methods. Human and mouse primary myoblasts were generated from human biopsy explants (provided by O.M. Dorchies, University of Geneva, Geneva, Switzerland), as described previously (44). Mitochondria were labeled with MitoTracker Red (CMXROS; Invitrogen) for 10 minutes. Samples were analyzed under a Leica DM microscope or a Leica SP2 MP confocal microscope.

Time-lapse microscopy. Cells incubated with MitoTraker Red were washed twice with culture medium prior to analysis. Cells were observed over 10 minutes using a Leica DMI6000 microscope (Leica Microsystems) coupled to a Yokogawa spinning-disc confocal unit CSU22 (Yokogawa Electric Corp.). Images were acquired by a back-illuminated EM-CCD camera (Andor iXon EM + DU-897; Andor Technology). Excitation was achieved with a solid-state laser (561 nm), and cells were maintained in a thermostatic chamber (Tokai Leica SP5 Super Z-Galvo Stage GSI; Tokai Hit) at 37°C with 5% CO_2. See Supplemental Methods for details of image analysis and mitochondrial tracking.

Electron microscopy. C2C12 *Mtm1*-KD and control cells were fixed with 2.5% (v/v) glutaraldehyde in 0.1M sodium cacodylate buffer (pH 7.2) for 24 hours at 4°C. Following washes in 0.1 M cacodylate buffer for 30 minutes, samples were postfixed in 1% osmium tetroxide in 0.1M cacodylate buffer for 1 hour at 4°C. Samples were dehydrated gradually by increasing concentrations of ethanol and embedded in Epon 812. Ultrathin sections (70 nm) were contrasted with uranyl acetate and lead citrate and observed with a Morgagni 268D electron microscope.

Muscle tissue preparation. *Mtm1*-KO and control male mice were euthanized by rapid cervical dislocation. Muscles were rapidly isolated and treated as described previously (45). Human biopsies were obtained in accordance with the French and European legislations following the written consent of all patients and control subjects. See Supplemental Methods for details.

Statistics. Data are mean ± SEM. Statistical analysis was performed using Mann-Whitney *U* test, unpaired 2-tailed Student's *t* test, or 1-way ANOVA followed by Bonferroni *t* test post-hoc correction. A *P* value less than 0.05 was considered significant. See Supplemental Methods for details.

Western and far-Western blot; peptides and dot blot; stable Mtm1-KD cell generation; generation of AAV-Mtm1 and intramuscular delivery; mitochondrial isolation; lipid binding assays; desmin solubility and phosphatase assays; cytochrome oxidase, LDH, and CK activities; cytochrome c release, MPT assay, and ATP content; apoptotic assays and JC-1 treatment; RT and quantitative PCR. See Supplemental Methods.

Acknowledgments

We acknowledge Christine Ruhlmann for the scanning transmission electron microscopy experiment; Olivier M. Dorchies for patient cells; Nadia Messaddeq for electron microscopy images; Christine Kretz for mouse genotyping; Nancy Monroy-Munoz, Pascal Eberling, Marc Koch, and Pascal Kessler for expert technical assistance; Olivier Pourquié and Olga Koutsopoulos for useful comments; and Fabrice Klein and Ali Poursaeed for illustrations. This study was supported by INSERM, CNRS, University of Strasbourg, and Collège de France and by grants from Association Française contre les Myopathies (AFM 11063, 12323, 12967, 13591, and 14204), Fondation Recherche Médicale (DEQ20071210538), E-rare program, GIS Institut Maladies Rares, and Agence Nationale de la Recherche (ANR-07-BLAN-0065-01 and ANR-08-GENOPAT-005). A.H. Beggs was supported by NIH grant P50 NS040828, the Joshua Frase Foundation, and the Lee and Penny Anderson Family Foundation. K.K. Tomczak was supported by a Research Development Grant from the Muscular Dystrophy Association. K. Hnia was supported by Collège de France and AFM.

Received for publication June 15, 2010, and accepted in revised form October 13, 2010.

Address correspondence to: Jocelyn Laporte, Institut de Génétique et de Biologie Moléculaire et Cellulaire, 1 Rue Laurent Fries, Illkirch 67404, France. Phone: 33.388653412; Fax: 33.388653201; E-mail: mtm@igbmc.fr.

1. Yang Y, Bauer C, Strasser G, Wollman R, Julien JP, Fuchs E. Integrators of the cytoskeleton that stabilize microtubules. *Cell*. 1999;98(2):229–238.
2. Huang JD, et al. Direct interaction of microtubule- and actin-based transport motors. *Nature*. 1999;397(6716):267–270.
3. Kim S, Coulombe PA. Intermediate filament scaffolds fulfill mechanical, organizational, and signaling functions in the cytoplasm. *Genes Dev*. 2007;21(13):1581–1597.
4. Toivola DM, Tao GZ, Habtezion A, Liao J, Omary MB. Cellular integrity plus: organelle-related and protein-targeting functions of intermediate filaments. *Trends Cell Biol*. 2005;15(11):608–617.
5. Fuchs E, Cleveland DW. A structural scaffolding of intermediate filaments in health and disease. *Science*. 1998;279(5350):514–519.
6. Coulombe PA, Wong P. Cytoplasmic intermediate filaments revealed as dynamic and multipurpose scaffolds. *Nat Cell Biol*. 2004;6(8):699–706.
7. Omary MB, Coulombe PA, McLean WH. Intermediate filament proteins and their associated diseases. *N Engl J Med*. 2004;351(20):2087–2100.
8. Milner DJ, Mavroidis M, Weisleder N, Capetanaki Y. Desmin cytoskeleton linked to muscle mitochondrial distribution and respiratory function. *J Cell Biol*. 2000;150(6):1283–1298.
9. Kostareva A, et al. Mice expressing L345P mutant desmin exhibit morphological and functional changes of skeletal and cardiac mitochondria. *J Muscle Res Cell Motil*. 2008;29(1):25–36.
10. Winter L, Abrahamsberg C, Wiche G. Plectin isoform 1b mediates mitochondrion-intermediate filament network linkage and controls organelle shape. *J Cell Biol*. 2008;181(6):903–911.
11. Laporte J, et al. A gene mutated in X-linked myotubular myopathy defines a new putative tyrosine phosphatase family conserved in yeast. *Nat Genet*. 1996;13(2):175–182.
12. Blondeau F, Laporte J, Bodin S, Superti-Furga G, Payrastre B, Mandel JL. Myotubularin, a phosphatase deficient in myotubular myopathy, acts on phosphatidylinositol 3-kinase and phosphatidylinositol 3-phosphate pathway. *Hum Mol Genet*. 2000;9(15):2223–2229.
13. Taylor GS, Maehama T, Dixon JE. Inaugural article: myotubularin, a protein tyrosine phosphatase mutated in myotubular myopathy, dephosphorylates the lipid second messenger, phosphatidylinositol 3-phosphate. *Proc Natl Acad Sci U S A*. 2000;97(16):8910–8915.
14. Begley MJ, Taylor GS, Kim SA, Veine DM, Dixon JE, Stuckey JA. Crystal structure of a phosphoinositide phosphatase, MTMR2: insights into myotubular myopathy and Charcot-Marie-Tooth syndrome. *Mol Cell*. 2003;12(6):1391–1402.
15. Buj-Bello A, et al. AAV-mediated intramuscular delivery of myotubularin corrects the myotubular myopathy phenotype in targeted murine muscle and suggests a function in plasma membrane homeostasis. *Hum Mol Genet*. 2008;17(14):2132–2143.
16. Tronchere H, et al. Production of phosphatidylinositol 5-phosphate by the phosphoinositide 3-phosphatase myotubularin in mammalian cells. *J Biol Chem*. 2004;279(8):7304–7312.
17. Laporte J, Liaubet L, Blondeau F, Tronchere H, Mandel JL, Payrastre B. Functional redundancy in the myotubularin family. *Biochem Biophys Res Commun*. 2002;291(2):305–312.
18. Dowling JJ, et al. Loss of myotubularin function results in T-tubule disorganization in zebrafish and human myotubular myopathy. *PLoS Genet*. 2009;5(2):e1000372.
19. Perrot R, Julien JP. Real-time imaging reveals defects of fast axonal transport induced by disorganization of intermediate filaments. *FASEB J*. 2009;23(9):3213–3225.
20. Al-Qusairi L, et al. T-tubule disorganization and defective excitation-contraction coupling in muscle fibers lacking myotubularin lipid phosphatase. *Proc Natl Acad Sci U S A*. 2009;106(44):18763–18768.
21. Suen DF, Norris KL, Youle RJ. Mitochondrial dynamics and apoptosis. *Genes Dev*. 2008;22(12):1577–1590.
22. Laporte J, Blondeau F, Gansmuller A, Lutz Y, Vonesch JL, Mandel JL. The PtdIns3P phosphatase myotubularin is a cytoplasmic protein that also localizes to Rac1-inducible plasma membrane ruffles. *J Cell Sci*. 2002;115(pt 15):3105–3117.
23. Biancalana V, et al. Characterisation of mutations in 77 patients with X-linked myotubular myopathy, including a family with a very mild phenotype. *Hum Genet*. 2003;112(2):135–142.
24. Goldfarb LG, Dalakas MC. Tragedy in a heartbeat: malfunctioning desmin causes skeletal and cardiac muscle disease. *J Clin Invest*. 2009;119(7):1806–1813.
25. Laporte J, et al. MTM1 mutations in X-linked myotubular myopathy. *Hum Mutat*. 2000;15(5):393–409.
26. Herrmann H, Strelkov SV, Burkhard P, Aebi U. Intermediate filaments: primary determinants of cell architecture and plasticity. *J Clin Invest*. 2009;119(7):1772–1783.
27. Perng MD, Wen SF, van den IP, Prescott AR, Quinlan RA. Desmin aggregate formation by R120G alphaB-crystallin is caused by altered filament interactions and is dependent upon network status in cells. *Mol Biol Cell*. 2004;15(5):2335–2346.
28. Vicart P, et al. A missense mutation in the alphaB-crystallin chaperone gene causes a desmin-related myopathy. *Nat Genet*. 1998;20(1):92–95.
29. Bar H, Strelkov SV, Sjoberg G, Aebi U, Herrmann H. The biology of desmin filaments: how do mutations affect their structure, assembly, and organisation? *J Struct Biol*. 2004;148(2):137–152.
30. Colakoglu G, Brown A. Intermediate filaments

exchange subunits along their length and elongate by end-to-end annealing. *J Cell Biol*. 2009; 185(5):769–777.
31. Kreplak L, Bar H, Leterrier JF, Herrmann H, Aebi U. Exploring the mechanical behavior of single intermediate filaments. *J Mol Biol*. 2005;354(3):569–577.
32. Helfand BT, Chang L, Goldman RD. Intermediate filaments are dynamic and motile elements of cellular architecture. *J Cell Sci*. 2004;117(pt 2):133–141.
33. Chang L, et al. The dynamic properties of intermediate filaments during organelle transport. *J Cell Sci*. 2009;122(pt 16):2914–2923.
34. Robinson FL, Dixon JE. Myotubularin phosphatases: policing 3-phosphoinositides. *Trends Cell Biol*. 2006;16(8):403–412.
35. Nicot AS, Laporte J. Endosomal phosphoinositides and human diseases. *Traffic*. 2008;9(8):1240–1249.
36. Tsujita K, et al. Myotubularin regulates the function of the late endosome through the gram domain-phosphatidylinositol 3,5-bisphosphate interaction. *J Biol Chem*. 2004;279(14):13817–13824.
37. Dang H, Li Z, Skolnik EY, Fares H. Disease-related myotubularins function in endocytic traffic in Caenorhabditis elegans. *Mol Biol Cell*. 2004; 15(1):189–196.
38. Herman GE, Finegold M, Zhao W, de Gouyon B, Metzenberg A. Medical complications in long-term survivors with X-linked myotubular myopathy. *J Pediatr*. 1999;134(2):206–214.
39. Bar H, et al. Conspicuous involvement of desmin tail mutations in diverse cardiac and skeletal myopathies. *Hum Mutat*. 2007;28(4):374–386.
40. Rezniczek GA, et al. Plectin 1f scaffolding at the sarcolemma of dystrophic (mdx) muscle fibers through multiple interactions with beta-dystroglycan. *J Cell Biol*. 2007;176(7):965–977.
41. Herrmann H, Aebi U. Intermediate filament assembly: fibrillogenesis is driven by decisive dimer-dimer interactions. *Curr Opin Struct Biol*. 1998;8(2):177–185.
42. Herrmann H, Aebi U. Intermediate filament assembly: temperature sensitivity and polymorphism. *Cell Mol Life Sci*. 1999;55(11):1416–1431.
43. Herrmann H, Haner M, Brettel M, Ku NO, Aebi U. Characterization of distinct early assembly units of different intermediate filament proteins. *J Mol Biol*. 1999;286(5):1403–1420.
44. Dorchies OM, et al. Normal innervation and differentiation of X-linked myotubular myopathy muscle cells in a nerve-muscle coculture system. *Neuromuscul Disord*. 2001;11(8):736–746.
45. Hnia K, et al. L-arginine decreases inflammation and modulates the nuclear factor-kappaB/matrix metalloproteinase cascade in mdx muscle fibers. *Am J Pathol*. 2008;172(6):1509–1519.